INRIA

Automatic Retrieval of Anatomical Structures in 3D Medical Images

Jérôme Declerck, Gérard Subsol, Jean-Philippe Thirion and Nicholas Ayache.

N° 2485

Février 1995

PROGRAMME 4

R apport de recherche

Automatic Retrieval of Anatomical Structures in 3D Medical Images

Jérôme Declerck, Gérard Subsol, Jean-Philippe Thirion and
Nicholas Ayache. *

Abstract: This paper describes a method to automatically generate the mapping between a completely labeled reference image and the 3D medical image of a patient. To achieve this, we combined three techniques: the extraction of 3D feature lines, their matching using 3D deformable line models, the extension of the deformation to the whole image space using warping techniques.

We present experimental results for the segmentation of structures in Magnetic Resonance images of the brain of different patients; the segmentation of the cortical and ventricle structures. We emphasize the advantages of using crest lines deformable models prior to surface based models. This gives a sparser representation of the data, easier to manipulate, and which makes the convergence of the model much less sensitive to initial positionning.

In the future, we hope to use this method to generate anatomical atlases, by the automatic interpretation of large sets of 3D medical images.

Key-words: deformable model, electronic atlas, feature line, non-rigid matching, warping.

(Résumé : tsvp)

*E-mail: Nicholas.Ayache@sophia.inria.fr
**http://www.inria.fr/Equipes/EPIDAURE-eng.html

Détection Automatique de Structures Anatomiques dans les Images Médicales 3D

Résumé : Le présent rapport décrit une méthode pour identifier automatiquement des structures anatomiques dans une image 3D d'un patient à partir d'une image où ces mêmes structures sont complètement référencées. Pour ce faire, nous avons combiné trois techniques : l'extraction de lignes caractéristiques, leur mise en correspondance en utilisant des modèles déformables de ces lignes, l'extension de la déformation ainsi obtenue à l'image entière grâce à des techniques de déformation d'images.

Nous présentons des résultats expérimentaux sur des images par résonance magnétique de cerveaux de patients différents, en identifiant plus précisément les structures corticales et ventriculaires. Nous insistons sur les avantages d'utiliser des modèles déformables de lignes de crête plutôt que des modèles de surfaces : en effet, cette représentation des données est plus concise et plus facile à manipuler. De plus, la convergence du modèle est moins sensible au positionnement initial.

A l'avenir, nous espérons appliquer ce procédé pour générer des atlas anatomiques électroniques par l'interprétation automatique de grands ensembles d'images médicales 3D.

Mots-clé : modèles déformables, atlas électronique, ligne caractéristique, mise en correspondance non-rigide, déformation.

1   Introduction

It becomes needless to emphasize the advantages of electronic atlases versus conventional paper atlases. Many examples of such atlases are known, such as the Voxel-Man ([28], [17], [24]), following the pioneering work of Bajcsy [2] and Evans [21].

However, even if such atlases are available, and even if Computer Graphic techniques are sufficiently developed to manipulate and display those atlases in real time, there remains a crucial need for a theoretical framework and *automatic* tools to :

- Generate atlases from large data sets,

- Average among features and models to create reference patients,

- Analyze the variability of features between patients,

- Find correspondences between the image of any patient and the atlases.

This paper presents one possible approach to achieve some of those goals, usually referred to as a segmentation problem, for which a strong a-priori knowledge of the human anatomy can be used.

As in many image processing problems, there are usually two dual and complementary ways to explore, which are the region based and the feature based techniques. The first kind of methods concentrates on the voxel values inside the regions (see for example [10]), whereas the second one concentrates on the boundaries of those regions (see for example [13] for 2D cases), such as the interfaces between organs, or specific lines or points of those surfaces (see [38], [36]).

In the present paper, we concentrate on a feature line based technique to segment fully automatically the same organ in the images of different patients. We give first a global description of the method, which is then detailed into feature lines extraction using differential geometry, registration of lines using deformable models, and at last 3D space deformation using warping techniques. Finally, we present a practical example, which is the automatic extraction of the cortical and ventricle surfaces from the 3D Magnetic Resonance image of a patient.

2   A global description of the method

We believe very much in bootstraping techniques for atlas building: from an approximate description of a patient anatomy, or from existing electronic atlases or from a set of manually segmented 3D reference images, we hope to build automatically better average representations of the studied organs, usable for the re-interpretation of the reference images, or the analysis of a larger set of images. The key point here is of course the automatic inter-patient registration.

To simplify, let us start with a single reference image I_r, with an associated fully labeled image M_r, called map (figure 1): each voxel value of the map M_r specifies the type of a corresponding structure in the reference image I_r. We call *structure* a set of connected voxels of M_r having the same label. I_p is the image of a new patient to process.

We will suppose also that images I_r and I_p have been acquired with the same modality and parameter settings: their intensities are very similar.

To find the correspondence between I_p and the reference map M_r, we propose to find first the correspondence between I_p and I_r and then to deform the reference map M_r into a new map M_p, exactly superimposable to I_p.

2.1   The general scheme

More precisely, what we propose is:

- to automatically find and label crest lines in I_r, corresponding to the structures of M_r,

- to find automatically the corresponding lines in I_p,

- to find the correspondence $D_{p,r}$ between those sets of lines,

- to either deform individual structures, or the global map M_r into new structures or into a new map M_p, which is exactly superimposable to I_p. This step is achieved by applying a warping technique to M_r using the found correspondences (see [6], [14]).
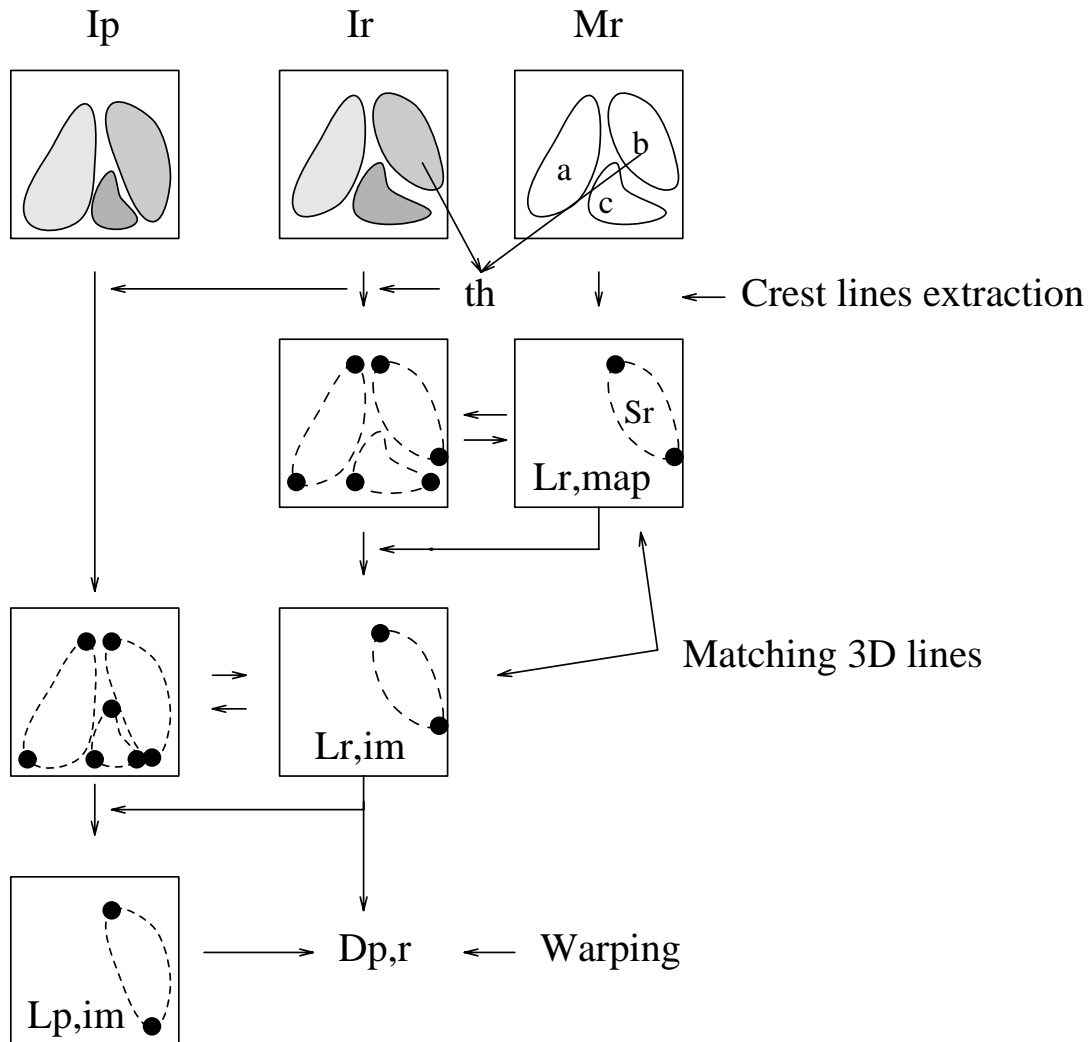
Figure 1: *Crest lines $L_{r,map}$ are extracted from the reference map and used to find the corresponding lines $L_{r,im}$ in the reference image I_r. The crest lines $L_{p,im}$ are extracted from the new image I_p, using $L_{r,im}$. This gives a set of correspondence and warping is applied to obtain the final deformation $D_{p,r}$*

2.2   The automatic labeling of crest lines

It is achieved structure by structure, fully automatically, in the following way (see also figure 1):

- Select one structure S_r of M_r (for example the ventricles of the brain).

- Extract the crest lines L_r^{map} of S_r (see [38]).

- Find the threshold th in I_r representative of the interface between S_r and the other structures, for example by computing the average value of the voxels of I_r in a region defined by the subtraction of the dilated and eroded versions of S_r (see [30]) for the definitions of those words).

- Extract the crest lines L_r^{im} in I_r imbedded in the iso-surface th.

- Register the two sets of crest lines L_r^{im} and L_r^{map} (see [18], [32]), to filter out from L_r^{im} the lines which have no correspondence in L_r^{map}.

The set of crest lines L_r^{im} is labeled with the name of the structure S_r.

2.3   The automatic retrieval of corresponding lines

We now search the corresponding lines L_p^{im} in the new image I_p:

- Extract the crest lines L_p^{im} of I_p within the iso-surface th (the hypothesis of similar dynamic of images is used here).

- Register L_p^{im} and L_r^{im}, and filter out from L_p^{im} the lines which have no correspondence in L_r^{im}.

At this point, we can compute a 3D B-spline approximation of a deformation $D_{p,r}$ between the two image spaces I_p and I_r. This can be achieved on one hand for each individual structure S_r, using the corresponding points between L_p^{im} and L_r^{im}. $D_{p,r}$ is then applied to S_r to obtain the structure S_p which is superimposable to I_p. On the other hand, this can be applied to the global map M_r, using simultaneously all structures, to deform M_r into M_p, the new map of image I_p.

3 Feature based non-rigid registration

This part describes the automatic extraction and deformable registration of crest lines.

3.1 The feature type

Raw medical images are stored in a discrete 3D matrix $I = f(x, y, z)$. By thresholding I, isosurfaces of organs are computed (for instance, the surface of the skull for CT-Scan, of the brain or the face for MRI). The problem, then, is to compute specific features of these surfaces. Several methods have been proposed to achieve this:

- *surface features* : the mean and Gaussian curvatures are used to segment the isosurface into patches of some fundamental types. Such a decomposition permits to study the deformations of the left ventricle [16] or to describe the faces [9].

- *line features* : Hosaka [20] reports a wide range of characteristic lines based on differential geometry. The 3D Medial Axis Transform gives also sets of lines, charting for instance the gyral anatomy [33].

- *point features* : the "extremal points" [37], based on geometric invariants are used to perform 3D rigid registration.

A first example of clinical application can be found in Cutting et al. [12], where line and point features are both used to compute "an average" skull. In that study, however, the features are manually extracted.

3.2 The crest lines

As explained before, we choose to use only line features: the crest lines introduced in [22]. They are defined as the successive loci of a surface for which the largest principal curvature is locally maximal in the principal direction (see figure 2). Let k_1 be the principal curvature with maximal curvature in
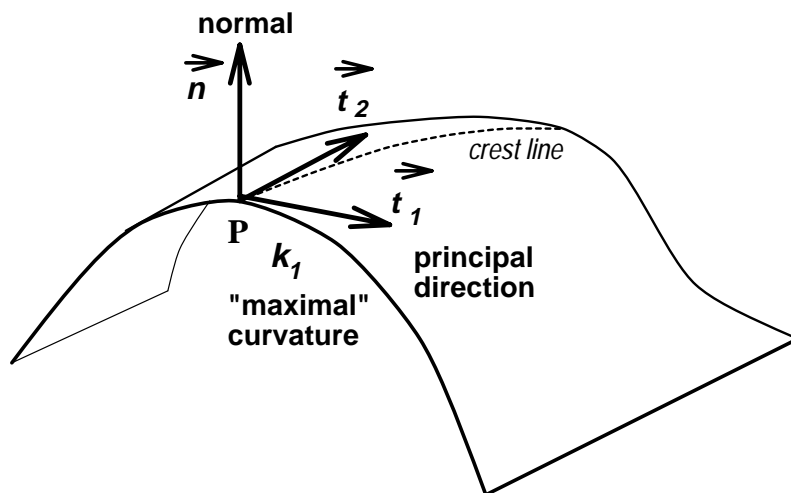
Figure 2: *Differential characteristics of a surface and the crest line.*

absolute value and $\overrightarrow{t_1}$ the associated principal direction, each point of a crest line verifies: $\overrightarrow{\nabla} k_1 . \overrightarrow{t_1} = 0$.

These lines are automatically extracted from an isosurface by the "marching lines" algorithm [38].

As we can see in the figure 5, crest lines are anatomically meaningful: on the skull, the crest lines represent the salient lines (the orbits, the nose, the mandible or the temples) as emphasized in [7]; on the brain, the crest lines follow the convolutions, the sulci and the gyri patterns described in Ono et al. [25].

3.3   The 3D registration algorithm

The 3D curves registration algorithm is a key point in our scheme: given two sets A and A' composed of the crest lines L_i and L'_j extracted from images of two different patients, we want to find which lines L_i of A (or portions $P_{i,k}$) correspond to which lines L'_j (or portions $P_{j,l}$) of A' (see figure 3). Two difficulties arise: the number of lines of each set is quite large (several hundreds,

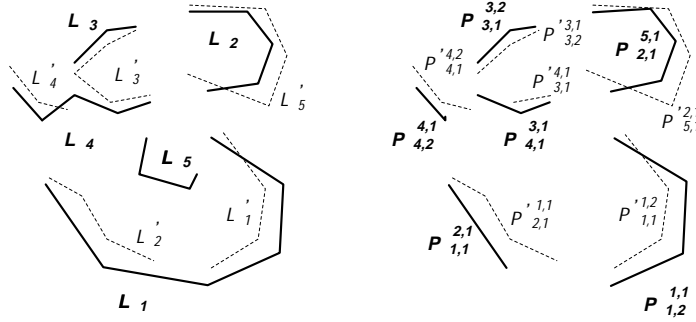sometimes more than a thousand) and the registration between A and A' is not rigid.

Figure 3: *The registration algorithm has to find the portions $P_{i,k}^{j,l}$ and $P_{j,l}^{'i,k}$, respectively the kth portion of L_i which corresponds to the lth portion of L_j and vice versa.*

In [3] and [29], 3D curves matching enables to recognize rigid synthetic objects. First, boundary curves are smoothed and then matched with prestored models but the registration is only rigid. In [18], the algorithm smoothes curves by using non-uniform B-splines. Then the two sets of curves are matched with a hashing table indexed by euclidean differential invariants. Results are very good [1] especially with sets of crest lines but the method only succeeds in finding a rigid displacement and cannot be generalized easily to the non-rigid case. Zhang in [39] and independently Besl [4] introduced an "iterative closest points" matching method (also generalized in [34]). It consists in three steps: for each point M_i of A, find the closest point M_i' of A'. Then, compute the global rigid displacement between the two sets of matched points $(M_1 \ldots M_n)$ and $(M_1' \ldots M_n')$ by a least-squares technique. Apply this motion to A and iterate until the motion is "small". Both authors use the algorithm to register free-form curves but once again for the rigid case. Nevertheless, we can improve and generalize this method to our problem.

Our algorithm follows the steps of the "iterative closest point" method.

3.3.1   Points matching

Each point of A is linked with its closest neighbour in A' according to the euclidean distance. We plan also to use in the distance computation the differential curve parameters as the tangent, normal, curvature and torsion [18] or surface parameters as the normal, the principal directions and principal curvatures as described in [15]. This gives two lists of registered points, $\mathcal{C}_1$.

But as we have curves, i.e. an *ordered* list of points, we can apply some topological constraints in order to remove no-consistent couples of linked points and to avoid the configurations of the figure 4 top where the line L_1 belongs to A and L_2 to A'.

With these couples of points $\mathcal{C}_2$, two coefficients are computed: p_i^j and $p_j'^i$ which are the proportion of the curve i of A matched with the curve j of A' and vice versa. Thus, by thresholding, $p_i^j \geq thr$ and $p_j'^i \geq thr$, we can determine the curves "registered" at thr percent. For instance, curves can be considered completely registered when $p_i^j \geq 0.5$ and $p_j'^i \geq 0.5$.

3.3.2   Least-squares transformation

We register A and A' with polynomial transformations. The 0th-order is a rigid transformation and 1st-order an affine transformation but they are not sufficient for satisfying non-rigid registration. So, we use 2nd-order polynomial transformations defined by:

$$\begin{cases} x' &= a_1x^2 &+a_2y^2 &+a_3z^2 &+a_4xy &+a_5yz &+a_6xz &+a_7x &+a_8y &+a_9z &+a_{10} \\ y' &= b_1x^2 &+b_2y^2 &+b_3z^2 &+b_4xy &+b_5yz &+b_6xz &+b_7x &+b_8y &+b_9z &+b_{10} \\ z' &= c_1x^2 &+c_2y^2 &+c_3z^2 &+c_4xy &+c_5yz &+c_6xz &+c_7x &+c_8y &+c_9z &+c_{10} \end{cases}$$

As these polynomials are linear in their coefficients, we can use the least-squares method [26], [5] to compute a_i, b_i and c_i.

Higher order polynomials may create large unexpected undulations as emphasized in [8]. 2nd-order polynomial transformations give accurate registration but we are not able to decompose them into intuitive physical meaning transformations such as rotation, translation or scaling. Notice that, at each iteration, we compose the transformation with a 2nd-order polynomial and so, we obtain after n iterations, a 2^n-order polynomial transformation. However,
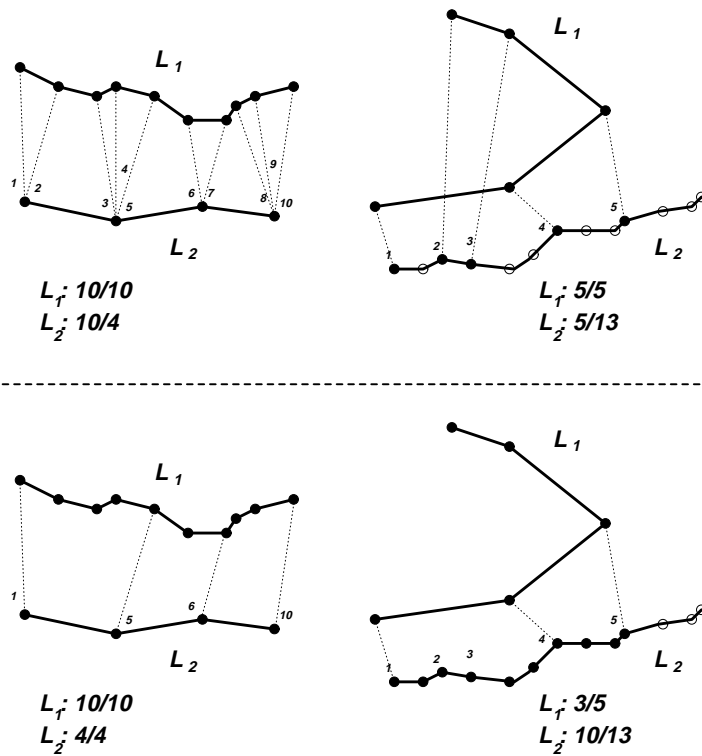
Figure 4: *The topological constraints help to remove inconsistent couples of linked points: left, some points have too many correspondents, right, a part of L_1 have a erroneous correspondent on L_2.*

such a iterative composition does not create the undulations [8] emphasizes: it seems that those undulations do not appear for such a class of polynomial transformations.

Such transformations are also used by Greitz et al. in [17] to model natural deformations as brain bending called scoliosis.

3.3.3   Updating

The transformation is applied, then the algorithm iterates again or stop according to several criteria (mean value of the distance distribution between matched points, stability of the registration coefficients p_i^j and $p_j^{\prime i}$, threshold on the matrix norm $||T - I_d||$ where T is the transformation and I_d the identity matrix).

3.3.4   Parameters adaptation

By incrementing the threshold value *thr* at each iteration, for instance, from 0 to 0.5 by step of 0.025 and by taking only into account the matched point couples (M, M') belonging to "registered" curves at *thr* percent, the algorithm tends to improve the registration of already matched curves and to discard isolated ones. Moreover, we can begin to apply rigid transformations to align the two sets of lines, then affine transformations to scale them and, at last, quadratic transformations to refine the registration.

At the end, we obtain a good registration between the two sets of lines and a point to point correpondence between lines; however, the transform is global, we need then to use a B-spline based warping technique to obtain a more local and a better approximation of the deformation.

4   Warping with B-splines

This section describes the method that has been developed to get a full superposition of two images (I_r and I_p), having a sparse set of corresponding points.

4.1   The problem

The process detailed in the previous section gives a set of pairs of points, each pair contains two matched points in both images. The aim of the following technique is to establish a matching on the whole images. Let us consider F as the matching function, this means a geometric transformation that, taking

a point in I_r, gives an anatomically equivalent point in I_p:

$$
\begin{array}{rccc}
F & : I_r & \longrightarrow & I_p \\
 & P_r & \longmapsto & P_p
\end{array}
$$

This function has obvious regularity properties.

A pair of points obtained with the above algorithm is hence an estimation of the pair $(P_r, F(P_r))$. Given the set of such pairs of landmarks, we have a partial knowledge of F, which will help us to define an estimation ϕ of it on the whole image. Having ϕ, it will be possible to warp the first image on the second.

4.2   Calculation of the warping function

A similar study has been proposed by Bookstein and Green ([6]), they calculate ϕ as a thin-plate spline interpolating function. We adopted a similar approach, but defining ϕ as an approximation of F rather than an interpolation.

4.2.1   The B-spline approximation

Let us consider (u, v, w) the coordinate functions of ϕ. We define them as a three-dimensional tensor product of B-spline basis functions:

$$
u(x, y, z) = \sum_{i=0}^{n_x-1} \sum_{j=0}^{n_y-1} \sum_{k=0}^{n_z-1} \alpha_{ijk}\, B_{i,K}^x(x)\, B_{j,K}^y(y)\, B_{k,K}^z(z)
$$

$$
v(x, y, z) = \sum_{i=0}^{n_x-1} \sum_{j=0}^{n_y-1} \sum_{k=0}^{n_z-1} \beta_{ijk}\, B_{i,K}^x(x)\, B_{j,K}^y(y)\, B_{k,K}^z(z)
$$

$$
w(x, y, z) = \sum_{i=0}^{n_x-1} \sum_{j=0}^{n_y-1} \sum_{k=0}^{n_z-1} \gamma_{ijk}\, B_{i,K}^x(x)\, B_{j,K}^y(y)\, B_{k,K}^z(z)
$$

with the following notations (for the x coordinate, for instance):

- n_x : the number of control points in the x direction. It controls the accuracy of the approximation.

- α : the 3D matrix of the control points abscissae. This is what we are looking for.

- $B_{i,K}^x$: the ith B-spline basis function. Its order is K. These $B_{i,K}^x$ generate the vectorial space of piecewise K^{th} degree polynomials. (see [27]). u is then a piecewise K^{th} degree polynomial in each variable x, y and z.

  We choose cubic B-splines in our examples ($K = 3$), for their regularity properties. For the knots, we took the classic regular mesh:

$$
\begin{aligned}
t_0^x &= ... = t_K^x = min_x \\
t_i^x &= min_x + (max_x - min_x)\,\frac{i - K}{n_x - K} \quad \text{for } K < i < n_x \\
t_{n_x}^x &= ... = t_{n_x + K}^x = max_x
\end{aligned}
$$

  where min_x and max_x are the boundaries of the definition domain (the image domain). The knots values can be optimized to get an accurate approximation, but the data are not that precise.

4.2.2 The constraints

We try to determine the best ϕ, with respect to our data. We then define three criteria J^x, J^y and J^z, one for each coordinate. For instance, for u, J^x splits in two parts:

- <u>position term</u>. For each data point, u taken on the point in the first image must be as close as possible to the abscissa of the corresponding point in the second image. We choose a least square criterion:

$$
J_{position}^x(u) = \sum_{l=1}^{N} \left(u(x_1^l, y_1^l, z_1^l) - x_2^l \right)^2
$$

which is developed as:

$$
J_{position}^x(u) = \sum_{l=1}^{N} \left(\sum_{i=0}^{n_x-1} \sum_{j=0}^{n_y-1} \sum_{k=0}^{n_z-1} \alpha_{ijk}\, B_{i,K}^x(x_1^l)\, B_{j,K}^y(y_1^l)\, B_{k,K}^z(z_1^l)\ -\ x_2^l \right)^2
$$

α_{ijk} is the 3D matrix of the control points abscissae, x_1^l the abscissa of the lth data point of the first image, etc...

- smoothing term. B-splines have intrinsic rigidity properties, but it is sometimes not enough. We choose a second order Tichonov stabilizer: it measures how far from an affine transformation the deformation is.

$$J_{smooth}^x(u) = \rho_{smooth} \int\int\int_{\mathbb{R}^3} \left[\frac{\partial^2 u}{\partial x^2}^2 + \frac{\partial^2 u}{\partial y^2}^2 + \frac{\partial^2 u}{\partial z^2}^2 + \frac{\partial^2 u}{\partial x \partial y}^2 + \frac{\partial^2 u}{\partial x \partial z}^2 + \frac{\partial^2 u}{\partial y \partial z}^2 \right]$$

where ρ_{smooth} is a balance coefficient. It is manually defined, some solutions to choose it automatically is currently studied. The integrals are calculated with the Gauss-Legendre algorithm, which gives exacts results for polynomials with very few evaluations of the integrand.

The criterion to minimize is the sum of those two:

$$J^x(u) = J_{position}^x(u) + J_{smooth}^x(u)$$

4.2.3   The linear systems

J is a positive quadratic function of the α_{ijk} variables. To find the coefficients that minimizes J^x, we derive its expression with respect to all the α_{ijk}: it gives $n_x.n_y.n_z$ linear equations which are written, for $0 \le a < n_x$, $0 \le b < n_y$ and $0 \le c < n_z$:

$$\sum_{i,j,k} \alpha_{ijk} \Big[\qquad \sum_{l=1}^N B_a^x(x_1^l)\, B_b^y(y_1^l)\, B_c^z(z_1^l)\, B_i^x(x_1^l)\, B_j^y(y_1^l)\, B_k^z(z_1^l)$$
$$+ \ \rho_{smooth} \ \left(I_{abc,ijk}^{xx} + I_{abc,ijk}^{yy} + I_{abc,ijk}^{zz} + 2\, I_{abc,ijk}^{xy} + 2\, I_{abc,ijk}^{xz} + 2\, I_{abc,ijk}^{yz} \right) \Big]$$
$$= \qquad \sum_{l=1}^N B_a^x(x_1^l)\, B_b^y(y_1^l)\, B_b^z(z_1^l)\, x_2^l$$

with shortening notations for the smoothing term:

$$I_{abc,ijk}^{xx} \ = \ \int\int\int_{\mathbb{R}^3} B''^x_a\, B^y_b\, B^z_c\, B''^x_i\, B^y_j\, B^z_k$$
$$I_{abc,ijk}^{xy} \ = \ \int\int\int_{\mathbb{R}^3} B'^x_a\, B'^y_b\, B^z_c\, B'^x_i\, B'^y_j\, B^z_k$$
$$\dots$$

Each integral is separable in a product of 3 simple integrals, they are hence easy to compute.

4.2.4   The resolution of the systems

The assembling of the matrix of the linear system is easy because this matrix is sparse: when all $B_{i,K}^x$ are evaluated for a given x, a maximum of K functions are non-zero (and then a minimum of $n_x - K$ is equal to zero). Moreover, the matrix is symmetric and positive, because the criterion is positive.

We use then a conjugate gradient method to solve our three systems (one for each coordinate).

4.3   Advantages of this warping method

The main advantages to compute B-splines are threefold:

- the B-splines functions are easy to evaluate with the Casteljau algorithm. The assembly of the matrices and the evaluation of the ϕ are then fast.

- the intrinsic rigidity properties of B-splines gives a regular function.

- a data point has a <u>local</u> influence : to evaluate an image of a point, we need only $(K + 1)^3$ control points (to be compared with the $n_x.n_y.n_z$ that have been calculated), those which are controlling the area around this point. Hence, the influence of outliers is very local.

5   Results and discussion

The data are presented on figures 6 and 7. On top, the reference brain extracted from I_r. Bottom, the patient brain extracted from I_p. Notice the differences of shapes and orientations; the patient brain is more compact than the reference brain, and it is rotated by a few degrees. The figure 7 shows the crest lines of the surfaces of the brains. The thin lines are those of the brain, the thick ones are those of the ventricle of each brain. Notice how different they are. These crest lines were the lines used in the registration algorithm.

On figure 8, the top line is the reference image I_r with the reference cortical surface S_r. The middle line is the image of the new patient I_p with the reference cortical surface S_r before deformation. The bottom line is the image I_p with the result S_p of the found deformation applied on S_r: see how it follows the

convolutions. The next figure shows a similar sequence with the surface of the ventricle.

The figure 10 helps to have on overall view of the deformation : it shows different 3D views of the reference brain (left) and the same brain after warping (right). The brains have been cut so that we can see the ventricles (the dark-grey structure) in their respective position.

The results are very good on that specific example, and they are encouraging in the perspective of a completely automatic registration process, given reference and patient images.

6   Conclusion and perspectives

The proposed method allows us to build fully automatically the maps associated to the 3D images of new patients, from manually designed maps of reference patients. It can be used to efficiently initialize 3D surface snakes if a more precise final segmentation of the organs is needed (see [11], [35]). The advantage of using crest lines prior to surface models is to have a much more compact representation, more easy to manipulate, that allows us to explore more numerous deformation hypotheses. Also, finding point to point correspondences between 3D lines is less ambiguous than between 3D surfaces, because lines are much sparser, and often correspond to anatomical landmarks. By having a very good starting point, and 3D structures whose topology is inferred directly from the reference maps, 3D surface snakes are more likely to converge toward the desired solution.

We are currently studying the integration of such 3D surface snakes into our method ([11]), in order to improve the quality of the automatically generated maps, and we develop also tools for averaging between patient features, and measuring variability (see [23], [32]). In the long run, we shall validate more thoroughly this study with a larger number of cases, and we plan to build tools for the automatic generation of anatomical atlases, using bootstraping.
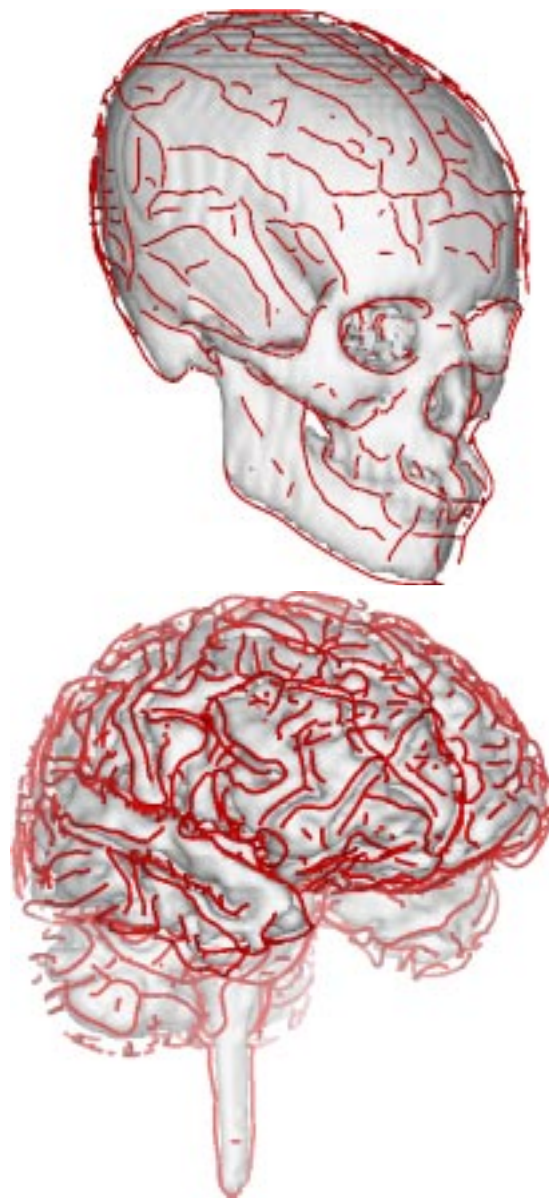
7   Acknowledgements

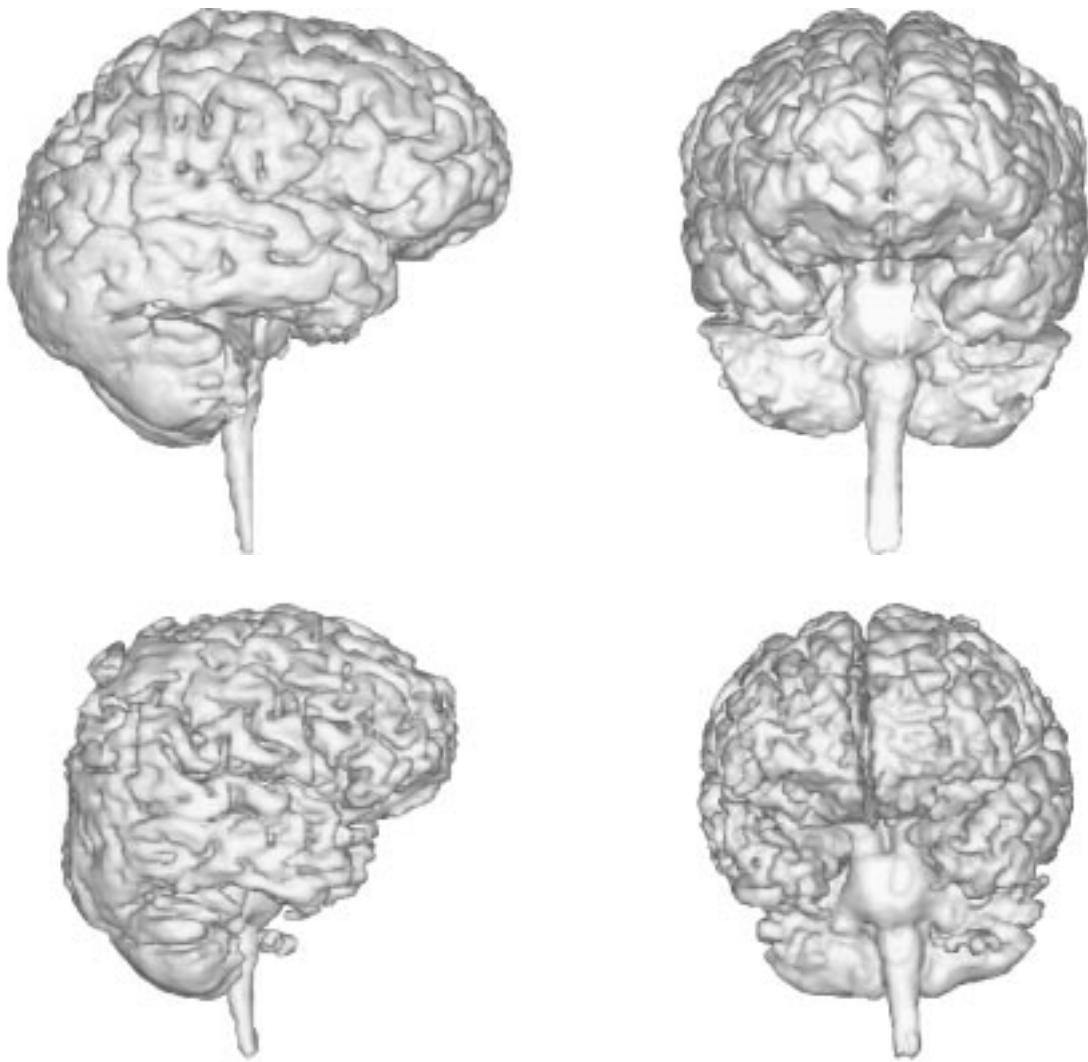Figure 5: *Crest lines of a skull and of a brain.*

Figure 6: *The data : top, the reference brain (the one which is warped), bottom, the patient brain. Notice the differences in shapes and orientations.*
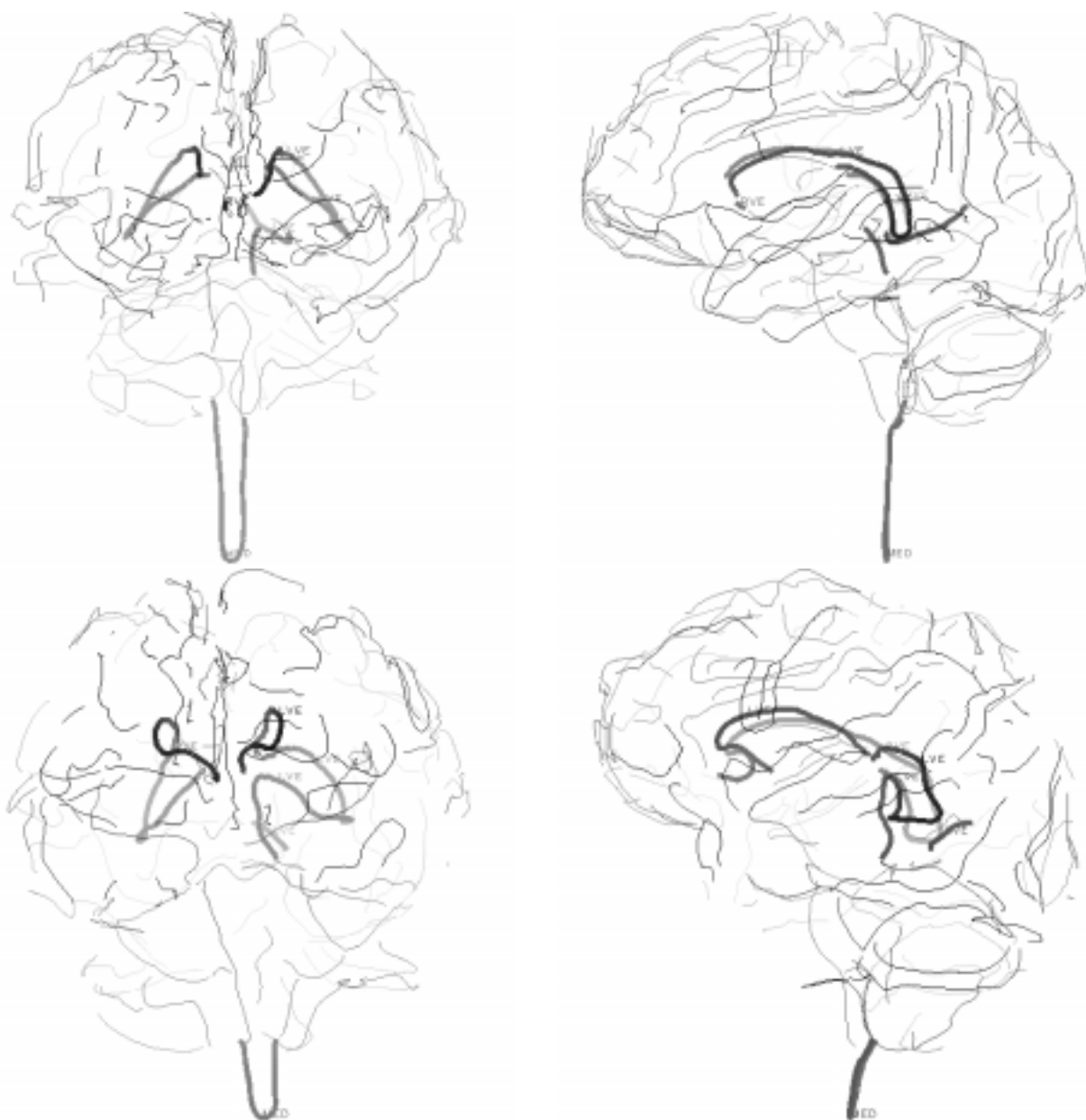
Figure 7: *The crest lines automatically extracted and labeled from the reference brain (top) and from the patient brain (bottom). The thick lines are those of the ventricle and of the medulla of each brain.*
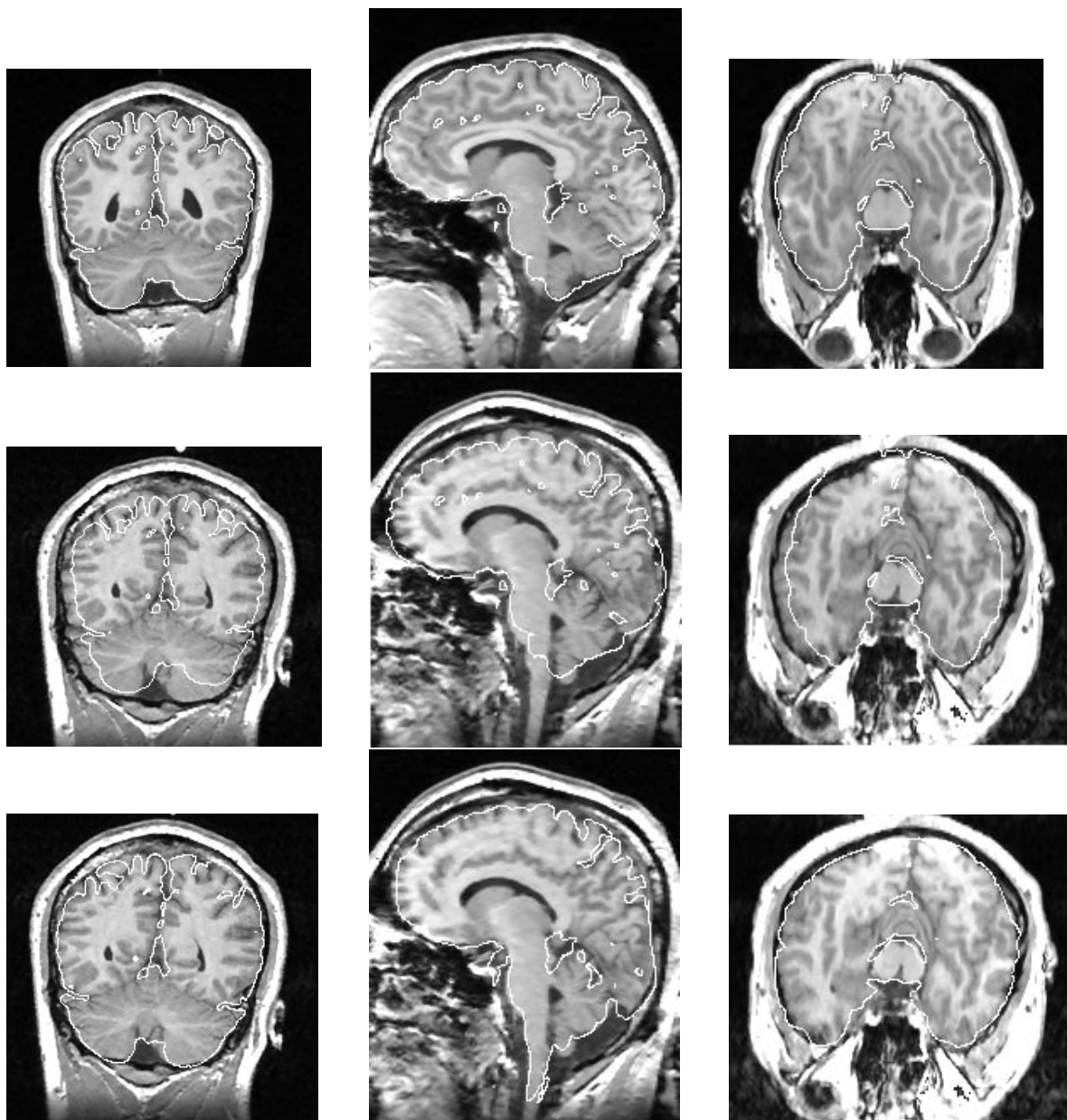
Figure 8: *Top line, the reference image I_r with the cortical surface S_r. Middle line, the patient image I_p with S_r before deformation. Bottom line, I_p with the result S_p of the found deformation applied on S_r.*
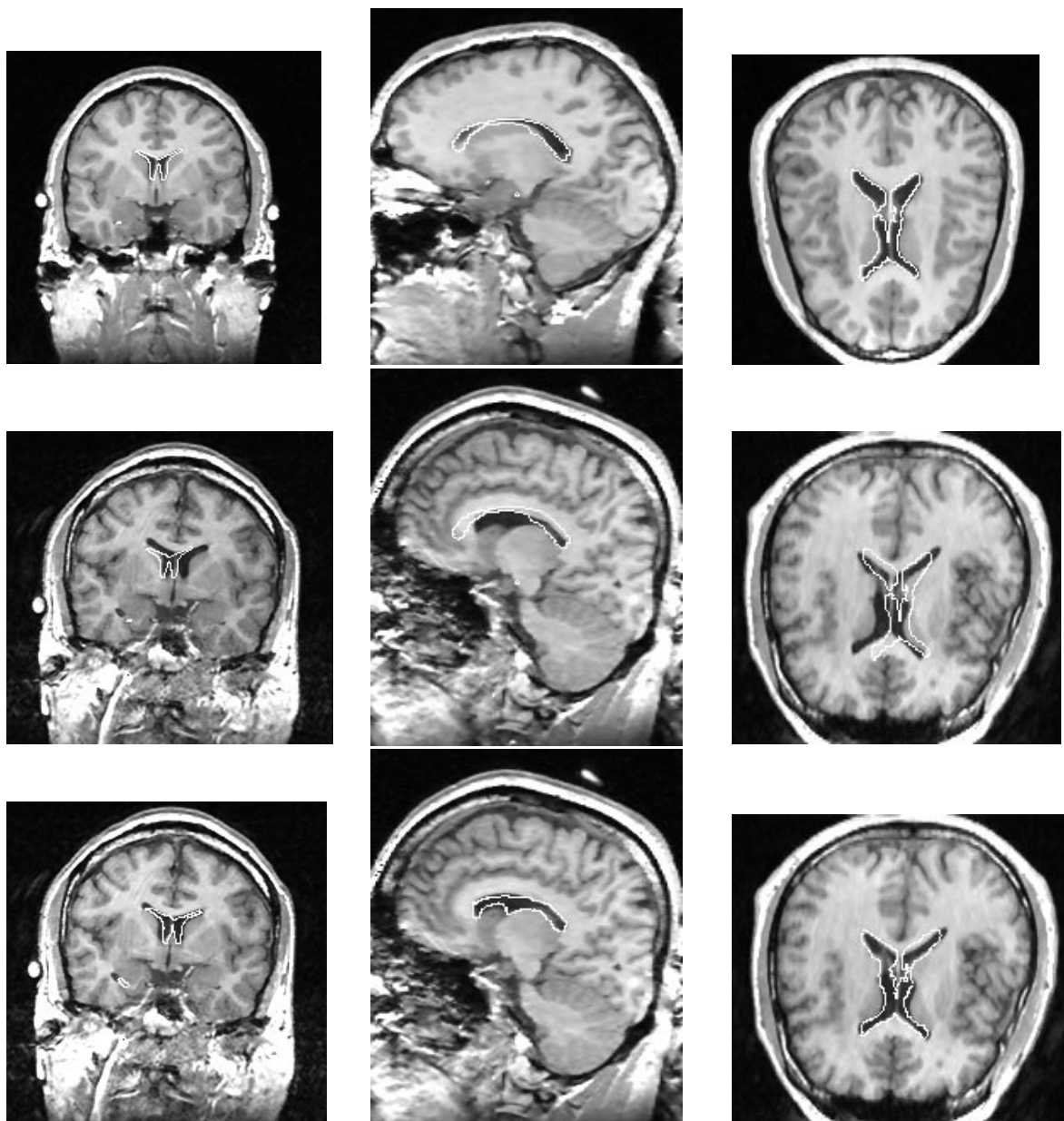
Figure 9: *Top line, the reference image I_r with the ventricle surface S_r. Middle line, the patient image I_p with S_r before deformation. Bottom line, I_p with the result S_p of the found deformation applied on S_r.*

Figure 10: *Different 3D views of the brains with their ventricle: left, the reference image, right, after warping.*

References

[1] N. Ayache, A. Guéziec, J.P. Thirion, A. Gourdon, and J. Knoplioch. Evaluating 3d registration of ct-scan images using crest lines. In David C. Wilson and Wilson Joseph N., editors, *Mathematical Methods in Medical Imaging II 1993*, pages 29–44, San Diego, California (USA), July 1993. SPIE.

[2] Ruzena Bajcsy and Stane Kovačič. Multiresolution Elastic Matching. *Computer Vision, Graphics and Image Processing*, (46):1–21, 1989.

[3] C. Marc Bastuscheck, Edith Schonberg, Jacob T. Schwartz, and Micha Sharir. Object recognition by three-dimensional curve matching. *International Journal of Intelligent Systems*, 1:105–132, 1986.

[4] Paul J. Besl and Neil D. McKay. A method for registration of 3-d shapes. *IEEE PAMI*, 14(2):239–255, February 1992.

[5] Å Björck. Algorithms for linear least squares problems. In Emilio Spedicato, editor, *Computer Algorithms for Solving Linear Algebraic Equations, the State of the Art*, pages 57–92. Springer-Verlag, 1991.

[6] F.L. Bookstein and W.D.K. Green. Edge information at landmarks in medical images. *SPIE Vol.1808*, 1992.

[7] Fred L. Bookstein and Court B. Cutting. A proposal for the apprehension of curving cranofacial form in three dimensions. In K. Vig and A. Burdi, editors, *Cranofacial Morphogenesis and Dysmorphogenesis*, pages 127–140. 1988.

[8] Lisa Gottesfeld Brown. A Survey of Image Registration Techniques. *ACM Computing Surveys*, 24(4):325–376, December 1992.

[9] Vicki Bruce, Anne Coombes, and Robin Richards. Describing the shapes of faces using surface primitives. *Image and Vision Computing*, 11(6):353–363, August 1993.

[10] Gary E. Christensen, Michael I. Miller, and Michael Vannier. A 3d deformable magnetic resonance textbook based on elasticity. In *AAAI symposium: Application of Computer Vision in Medical Image Processing*, pages 153–156, Stanford, March 1994.

[11] Isaac Cohen, Laurent Cohen, and Nicholas Ayache. Using deformable surfaces to segment 3D images and infer differential structures. In *CVGIP : Image understanding '92*, September 1992.

[12] Court B. Cutting, Fred L. Bookstein, Betsy Haddad, David Dean, and David Kum. A spline-based approach for averaging three-dimensional curves and surfaces. In David C. Wilson and Wilson Joseph N., editors, *Mathematical Methods in Medical Imaging II 1993*, pages 29–44, San Diego, California (USA), July 1993. SPIE.

[13] Chris Davatzikos and Jerry L. Prince. Brain image registration based on curve mapping. In *IEEE Workshop on Biomedical Image Analysis*, pages 245–254, Seattle, June 1994.

[14] Jérôme Declerck. Approximation de déformations géométriques par des B-splines. In *ECP, stage de fin d'études*, June 1993.

[15] Jacques Feldmar and Nicholas Ayache. Rigid and Affine Registration of Smooth Surfaces using Differential Properties. In *ECCV*, Stockholm (Sweden), May 1994. ECCV.

[16] Denis Friboulet, Isabelle E. Magnin, Andreas Pommert, and Michel Amiel. 3d curvature features of the left ventricle from ct volumic images. In *Information Processing in Medical Imaging*, pages 182–192. IPMI'92, 1992.

[17] Torgny Greitz, Christian Bohm, Sven Holte, and Lars Eriksson. A Computerized Brain Atlas: Construction, Anatomical Content and Some Applications. *Journal of Computer Assisted Tomography*, 15(1):26–38, 1991.

[18] A. Guéziec and N. Ayache. Smoothing and Matching of 3-D Space Curves. In *Visualization in Biomedical Computing*, pages 259–273, Chapel Hill, North Carolina (USA), October 1992. SPIE.

[19] K. Höhne, A. Pommert, M Riemer, T. Schiemann, R. Schubert, and U. Tiede. Framework for the generation of 3D anatomical atlases. In R. Robb, editor, *Visualization in Biomedical Computing*, volume 1808, pages 510–520. SPIE, 1992. Chapell Hill.

[20] M. Hosaka. *Modeling of Curves and Surfaces in CAD/CAM*. Springer-Verlag, 1992.

[21] S. Marrett, A. C. Evans, L. Collins, and T. M. Peters. A Volume of Interest (VOI) Atlas for the Analysis of Neurophysiological Image Data. In *Medical Imaging III: Image Processing*, volume 1092, pages 467–477. SPIE, 1989.

[22] Olivier Monga, Serge Benayoun, and Olivier D. Faugeras. Using Partial Derivatives of 3D Images to Extract Typical Surface Features. In *CVPR*, 1992.

[23] Chahab Nastar. Vibration Modes for Nonrigid Motion Analysis in 3D Images. In *Proceedings of the Third European Conference on Computer Vision (ECCV '94)*, Stockholm, May 1994.

[24] W.L. Nowinsky, A. Fang, B.T. Nguyen, R. Raghavan, R.N. Bryan, and J. Miller. Talairach-Tournoux / Schaltenbrand-Wahren Based Electronic Brain Atlas System. In Springer-Verlag, editor, *CVRMed*, April 1995.

[25] Michio Ono, Stefan Kubik, and Chad D. Abernathey. *Atlas of the Cerebral Sulci*. Georg Thieme Verlag, 1990.

[26] William H. Press, Brian P. Flannery, Saul A. Teukolsky, and Vettening William T. *Numerical Recipes in C, The Art of Scientific Computing*. Cambridge University Press, 1988.

[27] J.-J. Risler. *Méthodes Mathématiques Pour la CAO*. Masson, 1991.

[28] R. Schubert, K. H. Höhne, A. Pommert, M. Riemer, Th. Schiemann, and U. Tiede. Spatial knowledge representation for visualization of human anatomy and function. In H.H. Barrett and A.F. Gmitro, editors, *Information Processing in Medical Imaging*, pages 168–181, Flagstaff, Arizona (USA), June 1993. IPMI'93, Springer-Verlag.

[29] Jacob T. Schwartz and Sharir Micha. Identification of partially obscured objects in two and three dimensions by matching noisy characteristic curves. *The International Journal of Robotic Research*, 6(2):29–44, Summer 1987.

[30] J. Serra. *Image analysis and mathematical morphology*, volume 1. Academic Press, 1982.

[31] Gérard Subsol, Jean-Philippe Thirion, and Nicholas Ayache. First Steps Towards Automatic Building of Anatomical Atlases. Technical Report 2216, INRIA, March 1994.

[32] Gérard Subsol, Jean-Philippe Thirion, and Nicholas Ayache. Steps Towards Automatic Building of Anatomical Atlases. In *Visualization in Biomedical Computing '94*, October 1994.

[33] G. Székely, Ch. Brechbühler, O. Kübler, R. Ogniewicz, and T. Budinger. Mapping the human cerebral cortex using 3d medial manifolds. In Richard A. Robb, editor, *Visualization in Biomedical Computing*, pages 130–144, Chapel Hill, North Carolina (USA), October 1992. SPIE.

[34] R. Szeliski and S. Lavallée. Matching 3D Anatomical Surfaces with Non-Rigid Octree-Splines. In *IEEE Workshop on Biomedical Image Analysis*, pages 144–153, June 1994.

[35] D. Terzopoulos, A. Witkin, and M. Kaas. Constraints on deformable models : recovering 3D shape and non rigid motion. In *AI J.*, pages 91–123, 1988.

[36] J-P Thirion. Extremal points : definition and application to 3d image regist ration. In *IEEE conf. on Computer Vision and Pattern Recognition*, Seattle, June 1994.

[37] J.P. Thirion. New feature points based on geometric invariants for 3d image registration. Technical Report 1901, INRIA, May 1993.

[38] J.P. Thirion and A. Gourdon. The marching lines algorithm : new results and proofs. Technical Report 1881, INRIA, March 1993. to be published in CVGIP.

[39] Zhengyou Zhang. On Local Matching of Free-Form Curves. In David Hogg and Roger Boyle, editors, *British Machine Vision Conference*, pages 347–356, Leeds (United Kingdom), September 1992. British Machine Vision Association, Springer-Verlag.